sciendo

JAISCR, 2025, Vol. 15, No. 3, pp. 299 – 314
10.2478/jaiscr-2025-0015

NETWORK VIRUS PROPAGATION UNDER PLANAR CROSS-DIFFUSION: SPATIOTEMPORAL PATTERN ANALYSIS

Guangyong Zhang[1], Jiahui Zhang[2], Ludmila Dymova[3], Ying Zhou[2], Hua Li[2], Min Xiao[2,*]

[1]*Department of General Education, Wuxi University, 214105 Wuxi, China*

[2]*College of Automation & College of Artificial Intelligence, Nanjing University of Posts and Telecommunications, 210023 Nanjing, China*

[3]*Information Technology Institute, SAN University, 90-113 Łódź, Poland*

[*]*E-mail: candymanxm2003@aliyun.com*

Submitted: 3rd January 2025; Accepted: 2nd March 2025

Abstract

An important security problem faced by information networks is virus transmission. The traditional ordinary differential equation models of virus propagation take less consideration of the impact of diffusion factors in computer networks. A few reaction-diffusion models proposed to simulate virus spreading only take into account self-diffusion in one-dimensional space. As far as we know, there is not any model considering the cross-diffusion in two-dimensional space. In this paper, a novel virus transmission model with cross-diffusion in two-dimensional space is put forward. The introduction of cross-diffusion terms leads to diverse pattern dynamics and Turing instability in virus transmission, aspects that have not been previously studied. The sufficient conditions of Hopf bifurcation and Turing instability are given. Then, the amplitude equation near the critical value of Turing instability is constructed to identify various space-time patterns, such as spotted pattern, coexistence pattern and striped pattern. Finally, the numerical simulations show the correctness of theoretical analysis.

Keywords: cross-diffusion, turing instability, virus propagation, spatiotemporal pattern

1 Introduction

The rapid development of big data, cloud computing and artificial intelligence technology has pushed the Internet application to a new climax. However, network security concerns are becoming increasingly significant. Network virus is one of the main factors causing the problem of network security. In 2017, the ransomware virus broke out globally, affecting many industries such as energy, finance, healthcare, and education [3,19,29]. In daily operations, even if there is no large-scale virus outbreak, different types of network viruses such as Trojans, Distributed Deny of Service (DDoS) and botnets will constantly appear due to various interests, which attempt to destroy the normal operation of the Internet through various improper means [24]. Therefore, how to prevent, control or eliminate the spread of network viruses in the Internet has become a key issue.

In recent years, many scholars have established dynamic models considering different factors based

on ordinary differential equations (ODEs) to describe the characteristics of Internet virus transmission, and then predict the mechanism of virus transmission, and have made certain achievements [1, 20, 23, 32]. Among them, Feng et al. [7] considered a computer virus propagation model with double delay and proved that there is a critical value of delay for the stability of virus epidemic. Zhang et al. [30] proposed a delayed susceptible-exposed-infected-removed (SEIR) model for malware propagation in mobile wireless sensor networks, and studied the local stability and the occurrence of Hopf bifurcation. Liu and Zhang [18] investigated the epidemic model of worm propagation in wireless sensor networks with two incubation periods, and determined the propagation law of worms in mobile wireless sensor networks. However, the above literature only describes the time dynamic behavior of different nodes under the spread of network virus, but ignores or fails to predict the distribution of nodes in different spatial locations. It is worth noting that when network virus is injected into some nodes, the network virus may spread between nodes [12]. Some wireless network viruses can even spread through the air, such as Cabir and Comm Warrior [31]. Therefore, it is important to consider the mobility of nodes to study the spread of virus in the Internet and the distribution of nodes in different spatio-temporal regions.

In order to defend the damage of network virus, it is necessary to accurately understand the dynamic characteristics of virus propagation. Sabir et al. [22] presented a hybrid Particle Swarm Optimization (PSO) and Active-Set Algorithm (ASA) approach using Artificial Neural Network Procedures (ANNPs) to solve the SEIR model for Zika virus spread, optimized for accuracy and reliability. Avcl and Soyturk [2] proposed optimal control strategies to minimize antivirus installation costs while controlling virus spread in a network using a fractional-order SEIR model. Some mathematical models with self-diffusion terms have been introduced into network virus systems. The traditional virus transmission dynamics is promoted from time evolution to space-time evolution, and the mathematical model is extended from ODE to reaction-diffusion equation, which makes great progress in the research of virus spreading. For example, a reaction-diffusion malware propagation model with discrete time delay is proposed for mobile wireless sensor networks, and the sufficient conditions of the stability and Hopf bifurcation for the model are derived [33]. Zhu et al. [34] studied the Hopf bifurcation of virus propagation model in a class of delayed reaction-diffusion susceptible-infected-removed-susceptible (SIRS) network with feedback control. Significantly, they only consider the steady-state analysis of systems with self-diffusion terms in the one-dimensional spatial domain. Wang et al. [28] established a reaction-diffusion model for malware propagation, and discussed the temporal dynamic behavior and spatial distribution of malware propagation in wireless sensor networks. However, they only focus on the influence of the self-diffusion coefficient on the Turing spot of the infected nodes in the two-dimensional spatial domain.

It should be noted that current modeling research on virus propagation dynamics is based on ODEs, and it is more practical to take into account the diffusion effect. On the other hand, the existing reaction-diffusion models are limited to the self-diffusion and one-dimensional space diffusion, and ignore the cross diffusion and the diffusion in two-dimensional plane. As we know, diffusion may make the stable equilibrium point unstable and lead to non-uniform spatiotemporal patterns. Pattern dynamics has been widely studied in chemistry, biology and other fields [4, 6, 10, 11, 14, 15, 17, 26, 27]. One of the most classical models is the activator-inhibitor model proposed by Gierer and Meinhardt [8]. In addition, Li et al. [16] proposed the predator-prey model with cross-diffusion, and proved that Turing instability and cross-diffusion can produce spatiotemporal oscillatory solutions, which can enrich the formation of patterns in ecology. Despite extensive research on Turing spots, the pattern dynamics of virus transmission is rarely studied. However, the distribution pattern on the plane is more realistic and practical for the network system, which represents the distribution of different nodes. Moreover, the pattern on two-dimensional plane is more complicated than that on one-dimensional line. Only spot and stripe patterns exist in the one-dimensional space. In addition to spots and stripes, hexagonal patterns can also appear in two-dimensional space, and stripes and hexagons may coexist. It is helpful for us to accurately predict the dynamic behavior and spatial distribution of network virus spreading.

In a network system, nodes are mobile [28]. A susceptible node that enters the communication range of an infected node is highly susceptible to malware attacks. Similar to the spread of biological viruses from one organism to another, network viruses will also spread from infected nodes to non-infected nodes through various channels [9,28], and in some cases cause the malfunction of the network system. In the real network, the spatial structure of susceptible nodes and infected nodes also changes with time. Specifically, the two types of nodes influence each other, leading to changes in their spatial positions over time. Therefore, the self-diffusion and cross-diffusion factors are introduced in the modeling propagation process, which can reflect the interaction of internal network nodes. Especially, the influence on the spatial distribution of infected nodes has a very important practical significance, which can reflect the infection distribution in different spatio-temporal regions.)

Combined with the above, this paper establishes a network virus spreading model with cross-diffusion term in two-dimensional space. Analysis of stability and Turing instability is carried out by the linearization technique. Then the standard multi-scale analysis method is used to derive the amplitude equation around the critical value of Turing instability. By analyzing the amplitude equation, the pattern dynamics formed by the interaction between susceptible nodes and infected nodes can be obtained, such as the existence of uniform solutions, striped, hexagonal and mixed spot patterns and their stability. The described network virus propagation model is as follows:

$$\begin{cases} \dfrac{\partial u}{\partial t} = d_{11}\Delta u(t) + d_{12}\Delta v(t) + ru(1-\dfrac{u}{K}) \\ \qquad\quad -\dfrac{\beta uv}{u+v} + cv - \delta u, \\ \dfrac{\partial v}{\partial t} = d_{22}\Delta v(t) + \dfrac{\beta uv}{u+v} - dv - cv, \end{cases} \tag{1}$$

where $u(x,y,t),\ v(x,y,t)$ are the number of susceptible nodes and infected nodes in block (x,y) at instant t, respectively; $d_{11},\ d_{22}$ are respectively the self-diffusion coefficients of u and v, which are assumed to be positive; d_{12} is the cross-diffusion coefficient of the two nodes; The constant K is the carrying capacity the networks; r is the intrinsic increase rate of the network; β is the rate at which a susceptible node can become infected when it has a connection to an infected node; c is the recovery rate of infected nodes; δ, d are the death rates of susceptible nodes and infected nodes respectively.

For system (1), one takes the bounded domain $\Omega = [0,L_x] \times [0,L_y]$ in R^2 with the boundary $\partial\Omega$. $\Delta = \partial^2/\partial x^2 + \partial^2/\partial y^2$ is a commonly used Laplace operator in two-dimensional space, which is applied to describe the rate of change of the number of nodes in position (x,y) due to the movement behavior. Next, we investigate system (1) under the following initial conditions:

$$\begin{aligned} &u(x,y,0) = u_0(x,y) \geq 0, \\ &v(x,y,0) = v_0(x,y) \geq 0,\ (x,y) \in \Omega. \end{aligned}$$

We also assume that system (1) is subject to the Neumann boundary conditions

$$\frac{\partial u}{\partial n} = \frac{\partial v}{\partial n} = 0,\ (x,y) \in \partial\Omega,\ t \geq 0,$$

where n is the outward unit normal vector along $\partial\Omega$ and ∂n represents the operator of directional derivative along the direction n. The adoption of Neumann boundary conditions here means that the boundary of system (1) is zero flow vector.

The rest of this paper is organized as follows. In Section 2, we first study the stability of the internal constant steady state of system (1). In Section 3, we analyze the conditions under which the Turing instability of system (1) occurs using Neumann boundary conditions. In Section 4, we derive the amplitude equations using multiple scale analysis. In Section 5, we present a series of numerical simulations to reveal that system (1) can exhibit abundant spatiotemporal dynamics. Finally, some conclusions and discussions are given in Section 6.

2 Local stability and Hopf bifurcation

In this section, the stability of the equilibrium and the Hopf bifurcation are discussed to study the temporal dynamics of the non-spatial model. First, we give system (1) without diffusion terms as follows

$$\begin{aligned} \frac{du}{dt} &= ru(1-\frac{u}{K}) - \frac{\beta uv}{u+v} + cv - \delta u, \\ \frac{dv}{dt} &= \frac{\beta uv}{u+v} - dv - cv. \end{aligned} \tag{2}$$

We can obtain the following non-negative equilibrium points of the system (2):

1. $E_0 = (0,0)$, which is feasible;
2. $E_1 = (K(1-\frac{\delta}{r}),0)$, which is feasible;
3. $E_* = (u_*, v_*)$, where $u_* = \frac{mn-d\beta}{rn}$, $v_* = \frac{(\beta-d-c)u_*}{n}$, $m = r-\delta+d$, $n = d+c$.

According to the practical significance, this paper studies the only positive equilibrium point of system (2) as follows

$$E_* = (u_*, v_*) = (\frac{mn-d\beta}{rn}, \frac{(\beta-d-c)u_*}{n}),$$

where $m = r-\delta+d, n = d+c$, and $n < \beta < \frac{mn}{d}$.

We will study the local stability and Hopf bifurcation of the positive equilibrium point E_* of system (2). The Jacobian matrix corresponding to E_* is as follows

$$J = \begin{pmatrix} J_{11} & J_{12} \\ J_{21} & J_{22} \end{pmatrix}$$

where

$$J_{11} = r - \frac{2ru}{k} - \frac{\beta v^2}{(u+v)^2} - \delta, J_{12} = c - \frac{\beta u^2}{(u+v)^2},$$
$$J_{21} = \frac{\beta v^2}{(u+v)^2}, J_{22} = \frac{\beta u^2}{(u+v)^2} - d - c.$$

This leads to the characteristic equation as follows

$$\lambda_0^2 + Tr_0\lambda_0 + \Delta_0 = 0, \tag{3}$$

where

$$Tr_0 = -(J_{11}+J_{22}),\ \Delta_0 = J_{11}J_{22} - J_{12}J_{21}.$$

According to the Routh-Hurwitz criterion, if $J_{11}+J_{22} < 0$ and $J_{12}J_{21} - J_{11}J_{22} < 0$, the equilibrium point E_* is locally asymptotically stable.

Next, we select r as the bifurcation parameter. The critical value r_H of Hopf bifurcation can be obtained by solving the following equation

$$\begin{cases} Tr_0(r_H) = 0, \\ \Delta_0(r_H) > 0. \end{cases}$$

Let $\lambda_0(r) = x(r) + iy(r)$ represent the eigenvalue. Substitute it into (3) and separate the real and imaginary parts to get the following equation

$$\begin{cases} x^2 - y^2 + Tr_0 x + \Delta_0 = 0, \\ 2xy + Tr_0 y = 0. \end{cases} \tag{4}$$

Taking the derivative of (4) with respect to r, we can obtain

$$\begin{cases} 2x\frac{dx}{dr} - 2y\frac{dy}{dr} + \frac{dTr_0}{dr}x + \frac{d\Delta_0}{dr} + Tr_0\frac{dx}{dr} = 0, \\ 2y\frac{dx}{dr} + 2x\frac{dy}{dr} + \frac{dTr_0}{dr}y + Tr_0\frac{dy}{dr} = 0. \end{cases} \tag{5}$$

By solving (5) at $r = r_H$, we can get

$$\left.\frac{d\mathrm{Re}(\lambda_0)}{dr}\right|_{r_H} = \left.\frac{dx}{dr}\right|_{r_H} = \left.\frac{-2\frac{dTr_0}{dr}y^2 - Tr_0\frac{d\Delta_0}{dr}}{Tr_0^2 + 4y^2}\right|_{r_H}.$$

Therefore, the condition for the Hopf bifurcation of system (2) at the positive equilibrium point E_* is given by Theorem 1.

Theorem 1. For system (2), if there exists $r = r_H$ satisfying the following conditions, the system will have a Hopf bifurcation at the equilibrium point E_*.

1. $Tr_0(r_H) = 0$ and $\Delta_0(r_H) > 0$,
2. $\left.\frac{d\mathrm{Re}(\lambda_0)}{dr}\right|_{r_H} = \left.\frac{-2\frac{dTr_0}{dr}y^2 - Tr_0\frac{d\Delta_0}{dr}}{Tr_0^2 + 4y^2}\right|_{r_H} \neq 0.$

When r passes through r_H, the stability of the equilibrium E_* will switch. Assigning the values of r in the two sides of r_H, different dynamical behaviours such as asymptotical stability and oscillation can be observed in Figure 1, respectively. Here, we choose the parameters of system (2) as $K = 1, \beta = 0.5, d = 0.25, c = 0.001, \delta = 0.001$. The corresponding r_H is calculated as 0.2662.

3 Turing instability analysis

In this section, we analyze the linear stability of the space diffusion system (1), study the occurrence of Turing instability and give specific conditions.

First, the linearized form of system (1) about the interior equilibrium E_* is given as follows

$$\begin{cases} \frac{\partial \bar{u}}{\partial t} = d_{11}\nabla^2\bar{u} + d_{12}\nabla^2\bar{v} + J_{11}\bar{u} + J_{12}\bar{v}, \\ \frac{\partial \bar{v}}{\partial t} = d_{22}\nabla^2\bar{v} + J_{21}\bar{u} + J_{22}\bar{v}, \end{cases} \tag{6}$$

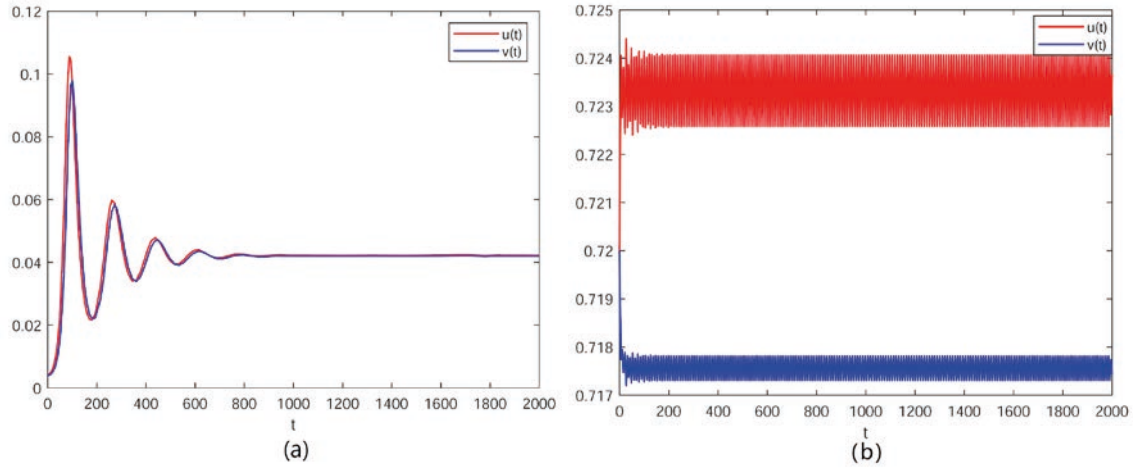


Figure 1. (a) When $r = 0.26$, which is less than the critical valve $r_H = 0.2662$, the equilibrium E_* of system (2) is asymptotically stable. (b) When $r = 0.90$, which is larger than the critical valve $r_H = 0.2662$, the dynamics of system (2) around the equilibrium E_* shows oscillatory behaviours.

where $u = u_* + \bar{u}, v = v_* + \bar{v}$, and $(\bar{u}, \bar{v})$ represents a perturbation of the system at the equilibrium point $E_* = (u_*, v_*)$. Next, we address the temporal stability of the uniform state to nonuniform perturbations

$$\begin{pmatrix} u \\ v \end{pmatrix} = \begin{pmatrix} u_* \\ v_* \end{pmatrix} + \varepsilon \begin{pmatrix} u_k \\ v_k \end{pmatrix} e^{\lambda t + ik\cdot r} + c.c., \quad (7)$$

where $k = (k_x, k_y), k \cdot k = k^2$, and k is the wave numbers. λ is the growth rate of perturbation in time t, and $r = (x, y)$ is the spatial vector in two-dimensional space.

Substituting (7) into system (1) and neglecting the higher order terms, we therefore obtain

$$\lambda \begin{pmatrix} A_k \\ B_k \end{pmatrix} = \begin{pmatrix} J_{11} - d_{11}k^2 & J_{12} - d_{12}k^2 \\ J_{21} & J_{22} - d_{22}k^2 \end{pmatrix} \begin{pmatrix} A_k \\ B_k \end{pmatrix}.$$

This leads to the dispersion relation as follows

$$\lambda^2 + Tr_k\lambda + \Delta_k = 0, \quad k \in \{0, 1, 2, ...\},$$

where

$$Tr_k = (d_{11} + d_{22})k^2 + Tr_0,$$
$$\Delta_k = d_{11}d_{22}k^4 + (J_{21}d_{12} - J_{11}d_{22} - J_{22}d_{11})k^2 + \Delta_0.$$

Turing instability occurs when the uniform steady state is stable in the system without the diffusion term, but unstable in the system with the diffusion term. Therefore, we assume $Tr_0 > 0$ and $\Delta_0 > 0$ to ensure that the equilibrium point E_* is locally stable in system (2). Since $d_{11} > 0$ and $d_{22} > 0$, it follows from the expression of Tr_k that $Tr_k > Tr_0 > 0$. At this point, the only case that leads to diffusion instability is $\Delta_k < 0$. Thus, the necessary conditions for Turing instability can be written as

$$\Delta_k = d_{11}d_{22}k^4 + (J_{21}d_{12} - J_{11}d_{22} - J_{22}d_{11})k^2 + \Delta_0 < 0.$$

Through analysis, we can find the minimum of Δ_k with respect to k^2. The most dangerous modulus value of the system to the perturbation is

$$k_c^2 = -\frac{J_{21}d_{12} - J_{11}d_{22} - J_{22}d_{11}}{2d_{11}d_{22}}.$$

Substituting the above formula back into Δ_k, the necessary condition for Turing instability to occur becomes

$$(\Delta_k)_{\min} = \Delta_0 - \frac{(J_{11}d_{22} + J_{22}d_{11} - J_{21}d_{12})^2}{4d_{11}d_{22}} < 0.$$

By solving the equation $(\Delta_k)_{\min} = 0$, we can obtain the critical value of r for the occurrence of instability, which is denoted by r_T. Based on the above analysis, the following theorem can be proposed.

Theorem 2. For system (1), if the following conditions hold, a Turing instability happens.

1. $Tr_0 > 0$ and $\Delta_0 > 0$,
2. $2\sqrt{d_{11}d_{22}\Delta_0} < J_{11}d_{22} + J_{22}d_{11} - J_{21}d_{12}$.

Remark 1. We prove that system (1) remains stable in the presence of self-diffusion but no cross-diffusion. From $Tr_0 > 0$, we know $J_{11} + J_{22} < 0$. Since $J_{11} + J_{22} < 0$, $\Delta_0 > 0, d_{11} > 0$ and $d_{22} > 0$, $2\sqrt{d_{11}d_{22}\Delta_0} < J_{11}d_{22} + J_{22}d_{11}$ is not established.

Therefore, there is no phenomenon of Turing instability in system (1) without cross-diffusion terms. This implies that the cross-diffusion is crucial for the appearance of Turing instability.

In order to verify the existence of Turing instability, we present a picture of the function Δ_k and the maximum real part $\mathrm{Re}(\lambda_k)$ of the eigenvalue as the wave number k^2 changes. The parameters used here in system (1) are $d_{11}=0.1, d_{12}=0.02, d_{22}=2, K=1, \beta=0.5, d=0.25, c=0.001, \delta=0.001$. We calculate the critical value $r_T=0.3226$ of Turing instability. Near the critical value, we set r as $0.3350, 0.3226, 0.3000, 0.2773$, and 0.2500. Figure 2(a) shows that with the increase of parameter r, the range of module k^2 that makes Δ_k negative gradually increases. Here, a wider range of k^2 implies a higher possibility for the occurrence of Turing instability. Figure 2(b) depicts the change of the maximum real part $\mathrm{Re}(\lambda_k)$ of the eigenvalue along with the change of k^2, showing the same trend as that of Figure 2(a). When $r > r_T$, the real part of λ_k becomes completely negative, which means the equilibrium E_* is stable in the spatial model (1). In this way, Turing instability cannot develop and pattern formation cannot form.

Remark 2. The parameter d_{12} represents the influence of infected nodes on the movement of susceptible nodes. When d_{12} is positive, the presence of infected nodes drives susceptible nodes away from high-infection regions, reflecting the repulsion effect in virus propagation [28].

Through the above analysis, the conditions of Turing pattern formation in system (1) are obtained. However, how to select the appropriate Turing structure remains a difficult problem. Therefore, in the following we will construct the amplitude equations near the critical values where Turing instability occurs and explain the stability of various forms of Turing diagrams and the structural transitions between them.

4 Amplitude equations of Turing patterns

In this section, we will derive the amplitude equation about the critical value at which Turing instability occurs by using standard multiscale analysis [5, 13, 21, 25]. The linearized form of the system (1) at the equipment $E_*=(u_*, v_*)$ is as follows, and perturbation $(u-u_*, v-v_*)^T$ is still denoted by $(u,v)^T$.

$$\begin{cases} \dfrac{\partial u}{\partial t} = d_{11}\nabla^2 u + d_{12}\nabla^2 v + J_{11}u + J_{12}v \\ \qquad + f_{uu}u^2 + f_{vv}v^2 + f_{uv}uv + f_{uuu}u^3 \\ \qquad + f_{vvv}v^3 + f_{uuv}u^2 v + f_{uvv}uv^2, \\ \dfrac{\partial v}{\partial t} = d_{22}\nabla^2 v + J_{21}u + J_{22}v + g_{uu}u^2 \\ \qquad + g_{vv}v^2 + g_{uv}uv + g_{uuu}u^3 + g_{vvv}v^3 \\ \qquad + g_{uuv}u^2 v + g_{uvv}uv^2, \end{cases} \tag{8}$$

where

$$\begin{aligned} f_{uu} &= -\frac{2r}{K} + \frac{2\beta v^2}{(u+v)^3},\ f_{uv} = \frac{-2\beta uv}{(u+v)^3}, \\ f_{vv} &= \frac{2\beta u^2}{(u+v)^3},\ f_{uuu} = \frac{-6\beta v^2}{(u+v)^4}, \\ f_{uuv} &= \frac{4\beta vu - 2\beta v^2}{(u+v)^4},\ f_{uvv} = \frac{4\beta vu - 2\beta u^2}{(u+v)^4}, \\ f_{vvv} &= \frac{-6\beta u^2}{(u+v)^4},\ g_{uu} = \frac{-2\beta v^2}{(u+v)^3}, \\ g_{uv} &= \frac{2\beta uv}{(u+v)^3},\ g_{vv} = \frac{-2\beta u^2}{(u+v)^3}, \\ g_{uuu} &= \frac{6\beta v^2}{(u+v)^4},\ g_{uuv} = \frac{-4\beta vu + 2\beta v^2}{(u+v)^4}, \\ g_{uvv} &= \frac{-4\beta vu + 2\beta u^2}{(u+v)^4},\ g_{vvv} = \frac{6\beta u^2}{(u+v)^4}. \end{aligned}$$

Set $U=(u,v)^T$, then (8) can be written as the following form

$$\frac{\partial U}{\partial t} = LU + F(U,U), \tag{9}$$

where L and F are the linear operator and nonlinear operator as follows

$$L = \begin{pmatrix} J_{11} + d_{11}\nabla^2 & J_{12} + d_{12}\nabla^2 \\ J_{21} & J_{22} + d_{22}\nabla^2 \end{pmatrix},$$

$$F = \begin{pmatrix} f_{uu}u^2 + f_{vv}v^2 + f_{uv}uv + f_{uuu}u^3 \\ \qquad + f_{vvv}v^3 + f_{uuv}u^2 v + f_{uvv}uv^2 \\ g_{uu}u^2 + g_{vv}v^2 + g_{uv}uv + g_{uuu}u^3 \\ \qquad + g_{vvv}v^3 + g_{uuv}u^2 v + g_{uvv}uv^2 \end{pmatrix}.$$

In the following, we decompose the operator L into the following form

$$L = L_T + (r_T - r)M, \tag{10}$$

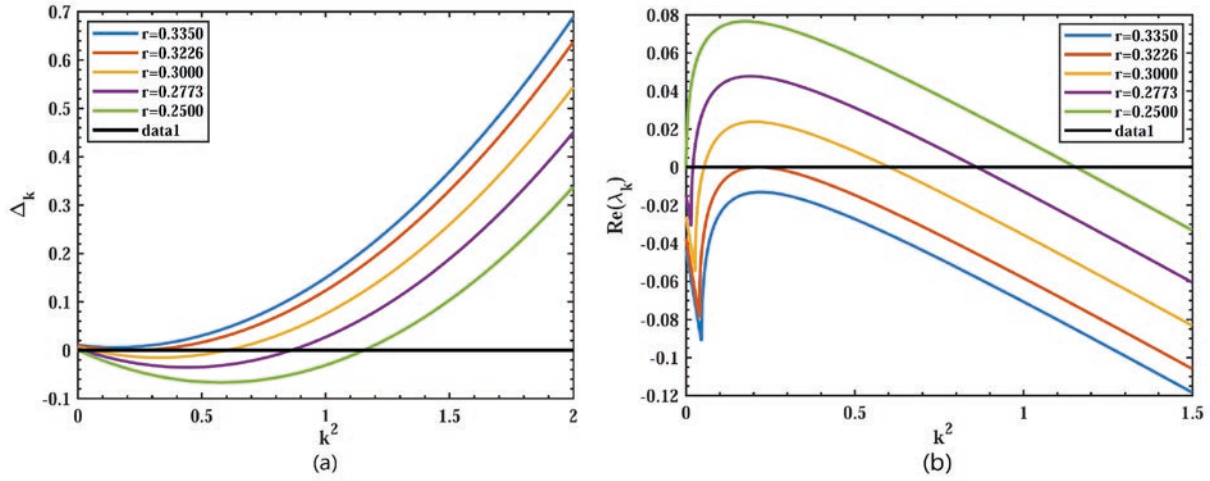


Figure 2. (a) Plots of Δ_k against k^2 for different values of parameter r. (b) Dispersion relation plotting the largest real part of the eigenvalues against k^2 for different values of parameter r.

where

$$L_T = \begin{pmatrix} J_{11}^T + d_{11}\nabla^2 & J_{12}^T + d_{12}\nabla^2 \\ J_{21}^T & J_{22}^T + d_{22}\nabla^2 \end{pmatrix},$$
$$M = \begin{pmatrix} m_{11} & m_{12} \\ m_{21} & m_{22} \end{pmatrix} \triangleq \begin{pmatrix} 1 & 0 \\ 0 & 0 \end{pmatrix},$$

in which

$$J_{ij}^T = J_{ij}|_{r=r_T}, m_{ij} = -\frac{dJ_{ij}}{dr}\bigg|_{r=r_T}, (i,j=1,2).$$

Further, parameter r, variable U and nonlinear term F are expanded according to small ε respectively as follows

$$r_T - r = \varepsilon r_1 + \varepsilon^2 r_2 + \varepsilon^3 r_3 + o(\varepsilon^3),$$
$$U = \begin{pmatrix} u \\ v \end{pmatrix} = \varepsilon \begin{pmatrix} u_1 \\ v_1 \end{pmatrix} + \varepsilon^2 \begin{pmatrix} u_2 \\ v_2 \end{pmatrix} + \varepsilon^3 \begin{pmatrix} u_3 \\ v_3 \end{pmatrix} + o(\varepsilon^3), \quad (11)$$
$$F = \varepsilon^2 F_2 + \varepsilon^3 F_3 + o(\varepsilon^3),$$

where

$$F_2 = \begin{pmatrix} f_{uu}{u_1}^2 + f_{vv}{v_1}^2 + f_{uv}u_1v_1 \\ g_{uu}{u_1}^2 + g_{vv}{v_1}^2 + g_{uv}u_1v_1 \end{pmatrix},$$
$$F_3 = \begin{pmatrix} m_{11} \\ m_{21} \end{pmatrix},$$

where

$$m_{11} = f_{uu}u_1u_2 + f_{uv}(u_1v_2 + u_2v_1) + f_{vv}v_1v_2 + f_{uuu}u_1^3 + f_{uuv}u_1^2v_1 + f_{uvv}u_1v_1^2 + f_{vvv}v_1^3,$$
$$m_{21} = g_{uu}u_1u_2 + g_{uv}(u_1v_2 + u_2v_1) + g_{vv}v_1v_2 + g_{uuu}u_1^3 + g_{uuv}u_1^2v_1 + g_{uvv}u_1v_1^2 + g_{vvv}v_1^3.$$

The time scale of the system is divided into three independent scales, and the derivative of time is obtained

$$\frac{\partial}{\partial t} = \frac{\partial}{\partial T_0} + \varepsilon\frac{\partial}{\partial T_1} + \varepsilon^2\frac{\partial}{\partial T_2} + o(\varepsilon^3), \quad (12)$$

where $T_0 = t$, $T_1 = \varepsilon t$, $T_2 = \varepsilon^2 t$.

By substituting the decomposition formulas (10), (11) into (12) and expanding (12) with respect to ε, we have the following equation for the order ε

$$\varepsilon : L_T \begin{pmatrix} u_1 \\ v_1 \end{pmatrix} = 0. \quad (13)$$

Similarly, we obtain the equations related to the orders ε^2 and ε^3

$$\varepsilon^2 : L_T \begin{pmatrix} u_2 \\ v_2 \end{pmatrix} = \frac{\partial}{\partial T_1}\begin{pmatrix} u_1 \\ v_1 \end{pmatrix} - r_1 M \begin{pmatrix} u_1 \\ v_1 \end{pmatrix} - F_2, \quad (14)$$

$$\varepsilon^3 : L_T \begin{pmatrix} u_3 \\ v_3 \end{pmatrix} = \frac{\partial}{\partial T_1}\begin{pmatrix} u_2 \\ v_2 \end{pmatrix} + \frac{\partial}{\partial T_2}\begin{pmatrix} u_1 \\ v_1 \end{pmatrix} - r_1 M \begin{pmatrix} u_2 \\ v_2 \end{pmatrix} - r_2 M \begin{pmatrix} u_1 \\ v_1 \end{pmatrix} - F_3. \quad (15)$$

Since L_T is a linear operator of the system at the critical point, $(u_1, v_1)^T$ is a linear combination of eigenvectors corresponding to zero eigenvalues of the solution of (13). We can write the modules

corresponding to the three wave vectors separately and obtain the general solution of (13) as follows

$$\begin{pmatrix} u_1 \\ v_1 \end{pmatrix} = \begin{pmatrix} \varphi \\ 1 \end{pmatrix} \left(\sum_{j=1}^{3} W_j \exp(ik_j \cdot r) + c.c. \right), \tag{16}$$

where $\varphi = \frac{d_{12}k_T^2 - J_{12}^T}{J^T - d_{11}k_T^2} = \frac{d_{22}k_T^2 - J_{22}^T}{J_{21}^T}$, $k_T = k_c(r_T)$. W_j is the amplitude of the mode $\exp(ik_j \cdot r)$ when the model is under the first order perturbation and its form is determined by the perturbational term of the higher order.

Next, for the existence of nontrivial solutions of (13) , according to the Fredholm solubility conditions, the right side of (13) should be orthogonal with the zero eigenvectors of L_T^* which is the adjoint operator of L_T. And the zero eigenvectors of L_T^* can be expressed as

$$\begin{pmatrix} 1 \\ \psi \end{pmatrix} \exp(-ik_j \cdot r) + c.c., j = 1,2,3,$$

where $\psi = \frac{d_{11}k_T^2 - J_{11}^T}{J_{21}^T} = \frac{d_{12}k_T^2 - J_{12}^T}{J_{22}^T - d_{22}k_T^2}$, According to orthogonal conditions and Fredholm solvability, we can get the amplitude equations under first order perturbation

$$\begin{cases} (\varphi+\psi)\dfrac{\partial W_1}{\partial T_1} = r_1 h_0 W_1 + 2(h_1 + \psi h_2)\overline{W}_2\overline{W}_3, \\ (\varphi+\psi)\dfrac{\partial W_2}{\partial T_1} = r_1 h_0 W_2 + 2(h_1 + \psi h_2)\overline{W}_1\overline{W}_3, \\ (\varphi+\psi)\dfrac{\partial W_3}{\partial T_1} = r_1 h_0 W_3 + 2(h_1 + \psi h_2)\overline{W}_1\overline{W}_2, \end{cases} \tag{17}$$

where

$$\begin{aligned} h_0 &= (\varphi m_{11} + m_{12}) + \psi(\varphi m_{21} + m_{22}), \\ h_1 &= f_{uu}\varphi^2 + f_{uv}\varphi + f_{vv}, \\ h_2 &= g_{uu}\varphi^2 + g_{uv}\varphi + g_{vv}. \end{aligned}$$

To ensure convergence, higher order perturbation terms are introduced. The solution of (14) can be obtained

$$\begin{aligned} \begin{pmatrix} u_2 \\ v_2 \end{pmatrix} = {} & \begin{pmatrix} U_0 \\ V_0 \end{pmatrix} + \sum_{j=1}^{3} \begin{pmatrix} U_j \\ V_j \end{pmatrix} \exp(ik_j \cdot r) \\ & + \sum_{j=1}^{3} \begin{pmatrix} U_{jj} \\ V_{jj} \end{pmatrix} \exp(2ik_j \cdot r) \\ & + \begin{pmatrix} U_{12} \\ V_{12} \end{pmatrix} \exp(i(k_1 - k_2) \cdot r) \\ & + \begin{pmatrix} U_{23} \\ V_{23} \end{pmatrix} \exp(i(k_2 - k_3) \cdot r) \\ & + \begin{pmatrix} U_{31} \\ V_{31} \end{pmatrix} \exp(i(k_3 - k_1) \cdot r) + c.c., \end{aligned} \tag{18}$$

By solving the equations corresponding to the different modes, we know that the coefficients have the following form

$$\begin{pmatrix} U_0 \\ V_0 \end{pmatrix} = \begin{pmatrix} u_{00} \\ v_{00} \end{pmatrix} \left(|W_1|^2 + |W_2|^2 + |W_3|^2\right), U_i = \varphi V_i,$$
$$\begin{pmatrix} U_{ii} \\ V_{ii} \end{pmatrix} = \begin{pmatrix} u_{11} \\ v_{11} \end{pmatrix} W_i^2, \begin{pmatrix} U_{kl} \\ V_{kl} \end{pmatrix} = \begin{pmatrix} u_{22} \\ v_{22} \end{pmatrix} W_k \overline{W}_l,$$

where the specific expression can be obtained by the undetermined coefficient method as

$$\begin{pmatrix} U_{00} \\ V_{00} \end{pmatrix} = \frac{-2}{J_{11}^T J_{22}^T - J_{21}^T J_{12}^T} \begin{pmatrix} J_{22}^T h_1 - J_{12}^T h_2 \\ J_{11}^T h_2 - J_{21}^T h_1 \end{pmatrix},$$

$$\begin{pmatrix} U_{11} \\ V_{11} \end{pmatrix} = \begin{pmatrix} \frac{-(J_{22}^T - 4d_{22}k_T^2)h_1 + (J_{12}^T - 4d_{12}k_T^2)h_2}{(J_{11}^T - 4d_{11}k_T^2)(J_{22}^T - 4d_{22}k_T^2) - (J_{12}^T - 4d_{12}k_T^2)J_{21}^T} \\ \frac{-(J_{11}^T - 4d_{11}k_T^2)h_2 + J_{21}^T h_1}{(J_{11}^T - 4d_{11}k_T^2)(J_{22}^T - 4d_{22}k_T^2) - (J_{12}^T - 4d_{12}k_T^2)J_{21}^T} \end{pmatrix},$$

$$\begin{pmatrix} U_{22} \\ V_{22} \end{pmatrix} = \begin{pmatrix} \frac{-2(J_{22}^T - 3d_{22}k_T^2)h_1 + 2(J_{12}^T - 3d_{12}k_T^2)h_2}{(J_{11}^T - 3d_{11}k_T^2)(J_{22}^T - 3d_{22}k_T^2) - (J_{12}^T - 3d_{12}k_T^2)J_{21}^T} \\ \frac{-2(J_{11}^T - 3d_{11}k_T^2)h_2 + 2J_{21}^T h_1}{(J_{11}^T - 3d_{11}k_T^2)(J_{22}^T - 3d_{22}k_T^2) - (J_{12}^T - 3d_{12}k_T^2)J_{21}^T} \end{pmatrix}.$$

Substituting $(u_2, v_2)^T$ into (15) and using Fredholm solvability conditions, we obtain the amplitude equations under first-order perturbation

$$\begin{cases} (\varphi+\psi)\left(\dfrac{\partial Y_1}{\partial T_1} + \dfrac{\partial W_1}{\partial T_2}\right) \\ = h_0(r_1 Y_1 + r_2 W_1) - [(I_1 + \psi I_3)|W_1|^2 \\ \quad + (I_2 + \psi I_4)(|W_2|^2 + |W_3|^2)]W_1 \\ \quad + (2h_1 + \psi h_2)(\overline{W}_2\overline{Y}_3 + \overline{W}_3\overline{Y}_2), \\ (\varphi+\psi)\left(\dfrac{\partial Y_2}{\partial T_1} + \dfrac{\partial W_2}{\partial T_2}\right) \\ = h_0(r_1 Y_2 + r_2 W_2) - [(I_1 + \psi I_3)|W_2|^2 \\ \quad + (I_2 + \psi I_4)(|W_1|^2 + |W_3|^2)]W_2 \\ \quad + (2h_1 + \psi h_2)(\overline{W}_1\overline{Y}_3 + \overline{W}_3\overline{Y}_1), \\ (\varphi+\psi)\left(\dfrac{\partial Y_3}{\partial T_1} + \dfrac{\partial W_3}{\partial T_2}\right) \\ = h_0(r_1 Y_3 + r_2 W_3) - [(I_1 + \psi I_3)|W_3|^2 \\ \quad + (I_2 + \psi I_4)(|W_2|^2 + |W_1|^2)]W_3 \\ \quad + (2h_1 + \psi h_2)(\overline{W}_2\overline{Y}_1 + \overline{W}_1\overline{Y}_2), \end{cases} \tag{19}$$

where

$$\begin{aligned} I_1 = {} & (2\varphi f_{uu} + f_{uv})(u_{00} + u_{11}) \\ & + (\varphi f_{uv} + 2f_{vv})(v_{00} + v_{11}) \\ & + 3(\varphi^3 f_{uuu} + \varphi^2 f_{uuv} + \varphi f_{uvv} + f_{vvv}), \\ I_2 = {} & (2\varphi f_{uu} + f_{uv})(u_{00} + u_{22}) \\ & + (\varphi f_{uv} + 2f_{vv})(v_{00} + v_{22}) \\ & + 6(\varphi^3 f_{uuu} + \varphi^2 f_{uuv} + \varphi f_{uvv} + f_{vvv}), \end{aligned}$$

$$
\begin{aligned}
I_3 &= (2\varphi g_{uu} + g_{uv})(u_{00} + u_{11}) \\
&\quad + (\varphi g_{uv} + 2g_{vv})(v_{00} + v_{11}) \\
&\quad + 3(\varphi^3 g_{uuu} + \varphi^2 g_{uuv} + \varphi g_{uvv} + g_{vvv}), \\
I_4 &= (2\varphi g_{uu} + g_{uv})(u_{00} + u_{22}) \\
&\quad + (\varphi g_{uv} + 2g_{vv})(v_{00} + v_{22}) \\
&\quad + 6(\varphi^3 g_{uuu} + \varphi^2 g_{uuv} + \varphi g_{uvv} + g_{vvv}).
\end{aligned}
$$

The amplitude $A_i = A_j^u = \varphi A_j^v$ is the coefficient of $\exp(iq_j \cdot r)$ in all levels and can be expanded as follows

$$A_j = \varepsilon W_j + \varepsilon^2 V_j + o(\varepsilon^3). \tag{20}$$

The derivative with respect to t can be expressed as follows

$$\frac{\partial A_j}{\partial t} = \varepsilon \frac{\partial A_j}{\partial t_1} + \varepsilon^2 \frac{\partial A_j}{\partial t_2} + o(\varepsilon^2). \tag{21}$$

Multiply (17) and (19) by ε and ε^2, respectively, and combine variables using (20) and (21) to get the following amplitude equations

$$
\begin{aligned}
\tau_0 \frac{\partial A_1}{\partial t} &= \mu A_1 + h\bar{A}_2\bar{A}_3 - [g_1|A_1|^2 + g_2(|A_2|^2 + |A_3|^2)]A_1, \\
\tau_0 \frac{\partial A_2}{\partial t} &= \mu A_2 + h\bar{A}_1\bar{A}_3 - [g_1|A_2|^2 + g_2(|A_1|^2 + |A_3|^2)]A_2, \\
\tau_0 \frac{\partial A_3}{\partial t} &= \mu A_3 + h\bar{A}_1\bar{A}_2 - [g_1|A_3|^2 + g_2(|A_1|^2 + |A_2|^2)]A_3,
\end{aligned}
$$

where

$$
\begin{aligned}
\mu &= \frac{r^T - r}{r},\ \tau_0 = \frac{\varphi + \psi}{r^T h_0},\ h = \frac{2(h_1 + \psi h_2)}{r^T h_0}, \\
g_1 &= -\frac{I_1 + \psi I_3}{r^T h_0},\ g_2 = -\frac{I_2 + \psi I_4}{r^T h_0}.
\end{aligned}
$$

Suppose that each amplitude in (20) could be decomposed as

$$A_j = \rho_j \exp(i\theta_j),\ j = 1,2,3. \tag{22}$$

Then substituting (22) into (20) and separating the real and imaginary parts, we can obtion

$$
\begin{aligned}
\tau_0 \frac{\partial \theta}{\partial t} &= -h\frac{\rho_1^2\rho_2^2 + \rho_1^2\rho_3^2 + \rho_2^2\rho_3^2}{\rho_1\rho_2\rho_3}\sin\theta, \\
\tau_0 \frac{\partial \rho_1}{\partial t} &= \mu\rho_1 + h\rho_2\rho_3\cos\theta - g_1\rho_1^3 - g_2(|\rho_2|^2 + |\rho_3|^2)\rho_1, \\
\tau_0 \frac{\partial \rho_2}{\partial t} &= \mu\rho_2 + h\rho_1\rho_3\cos\theta - g_1\rho_2^3 - g_2(|\rho_1|^2 + |\rho_3|^2)\rho_2, \\
\tau_0 \frac{\partial \rho_3}{\partial t} &= \mu\rho_3 + h\rho_2\rho_1\cos\theta - g_1\rho_3^3 - g_2(|\rho_1|^2 + |\rho_2|^2)\rho_3,
\end{aligned}
$$

where $\theta = \theta_1 + \theta_2 + \theta_3$.

By analyzing the amplitude equations, different modes of the reaction-diffusion system (1) and its stability can be obtained. The results of the correlation analysis are shown below.

1. Homogeneous stationary state:

   $$\rho_1 = \rho_2 = \rho_3 = 0,$$

   which is stable when $\mu < \mu_2 = 0$ and unstable when $\mu > \mu_2 = 0$.

2. Stripe pattern:

   $$\rho_1 = \sqrt{\frac{\mu}{g_1}} \neq 0,\ \rho_2 = \rho_3 = 0,$$

   which is stable when $\mu > \mu_3 = \frac{h^2 g_1}{(g_2 - g_1)^2}$ and unstable when $\mu < \mu_3$.

3. Spot pattern:

   $$\rho_1 = \rho_2 = \rho_3 = \frac{|h| \pm \sqrt{h^2 + 4(g_1 + 2g_2)\mu}}{2(g_1 + 2g_2)}.$$

   When $\mu > \mu_1 = \frac{-h^2}{4(g_1+2g_2)}$, there is a spot pattern. While $\mu < \mu_4 = \frac{(2g_1+g_2)h^2}{(g_2-g_1)^2}$, the solution $\rho^+ = \frac{|h|+\sqrt{h^2+4(g_1+2g_2)\mu}}{2(g_1+2g_2)}$ is stable and the other solution $\rho^- = \frac{|h|-\sqrt{h^2+4(g_1+2g_2)\mu}}{2(g_1+2g_2)}$ is always unstable.

4. Mixed structure state:

   $$\rho_1 = \frac{|h|}{g_2 - g_1},\ \rho_2 = \rho_3 = \sqrt{\frac{\mu - g_1\rho_1^2}{g_1 + g_2}}.$$

   It exists when $\mu > \mu_3$ and is always unstable with $g_2 > g_1$.

5 Numerical simulation

In this section, we present a numerical simulation of the speckle pattern of the diffusion system (1) in a two-dimensional plane to verify the correctness of the above theoretical analysis. To plot the distribution of susceptible nodes in a two-dimensional region, system (1) is numerically solved by the forward finite difference method with time step $\Delta t = 0.004$. Here, the two-dimensional domain is uniformly divided by 200×200 lattice points, and the boundary conditions we adopt are Neumann conditions. The simulation results show that the spatial pattern distribution of susceptible nodes and infected nodes is similar, so we present the numerical simulation results of susceptible nodes.

Table 1. Range of u with respect to different values of r.

r	h	g_1	g_2	μ_1	μ_2	μ_3	μ_4	μ
0.3000	4.0284	1130.5	2387.1	−0.001	0	0.0116	0.0478	0.0701
0.2773	19.0241	14.8118	972.88	−0.046	0	0.0058	0.3953	0.1404
0.2500	68.5568	2322.8	3931.3	−0.0115	0	0.4219	1.5880	0.1940

Next, we will conduct numerical simulation around the Turing bifurcation point. Firstly, the parameters of system (1) are set as follows: $d_{11} = 0.1, d_{12} = 0.02, d_{22} = 2, K = 1, \beta = 0.5, d = 0.25, c = 0.001, \delta = 0.001$. we calculated the Turing instability critical value of $r_T = 0.3226$. Secondly, we control the parameters r equal to 0.2500, 0.2773, and 0.3000 respectively to satisfy the condition of Turing instability. In order to make the theoretical analysis more intuitive, the value of r and the corresponding amplitude equation coefficients are listed in Table 1.

Figure 3 illustrates the spatial patch evolution of susceptible nodes in system (1). The subfigures correspond to the spatial structure with $3000, 22500, 42500, 70000, 100000$ and 150000 iterations, respectively. Here, we choose $r = 0.25$, and the other parameters of the model are consistent with the above, which can be calculated to obtain $\mu \in (\mu_2, \mu_3)$. According to the analysis of the theoretical results above, only spot patterns can exist in the final stable state of the system. As observed from Fig. 3, the pattern takes a long time to determine. With the development and diffusion of the perturbation, the system changes from the initial disorganized state to a mixture of spots and strips. Then, the strip structure gradually decays and the spot structure gradually increases in the system. Finally, more and more spot patterns are generated, occupying the entire two-dimensional plane. The numerical simulation shows the correctness of the theoretical analysis.

Figure 4 displays the pattern evolution of a mixture of strips and spots of susceptible nodes in system (1). The subgraph corresponds to the spatial structure of iteration times of $10000, 25000, 37500, 50000, 100000$ and 150000 respectively. Here we choose $r = 0.2773$ and $\mu \in (\mu_3, \mu_4)$. As shown in Fig. 4 the system is initially in a disordered transient state. Then, with the development of the density of susceptible nodes, the system gradually formed a mixture of strip and spot pattern. In this process, the spots and strips coalesce separately. Eventually, it evolved completely in shape and color, and distributed over the entire two-dimensional plane. The numerical simulation shown in Fig. 4 is consistent with the theoretical analysis.

Figure 5 shows the spatial structure of the susceptible nodes in system (1) that finally form the strips after iteration $2500, 10000, 25000, 37500, 100000$ and 150000 times. Here we choose $r = 0.3$ and the value of μ is greater than that of μ_4. It can be seen from Figure 5 that after the initial irregular state, the strip pattern appears. They smoothly cluster and intertwine with each other, eventually distributing over the entire two-dimensional plane. According to the theoretical analysis, the final stability result of the system is a strip pattern. This agrees with the theoretical analysis.

Remark 3. The model proposed in this study can be used to optimize network virus detection strategies. For example, when monitoring reveals that the node distribution exhibits a striped pattern (Figure 5), it indicates that the virus propagation has a directional tendency, and containment measures such as isolating high-infection-density regions can be implemented to curb the spread. Additionally, the coexistence of strip and spot pattern (Figure 4) suggests the need for dynamic adjustment of security strategies to address complex propagation pathways.

6 Conclusions

This study makes significant theoretical contributions by introducing cross-diffusion terms into a two-dimensional spatial framework for the first time, uncovering the intricate relationship between pattern dynamics and network virus propagation. The proposed model not only advances our understanding of spatiotemporal patterns in virus trans-

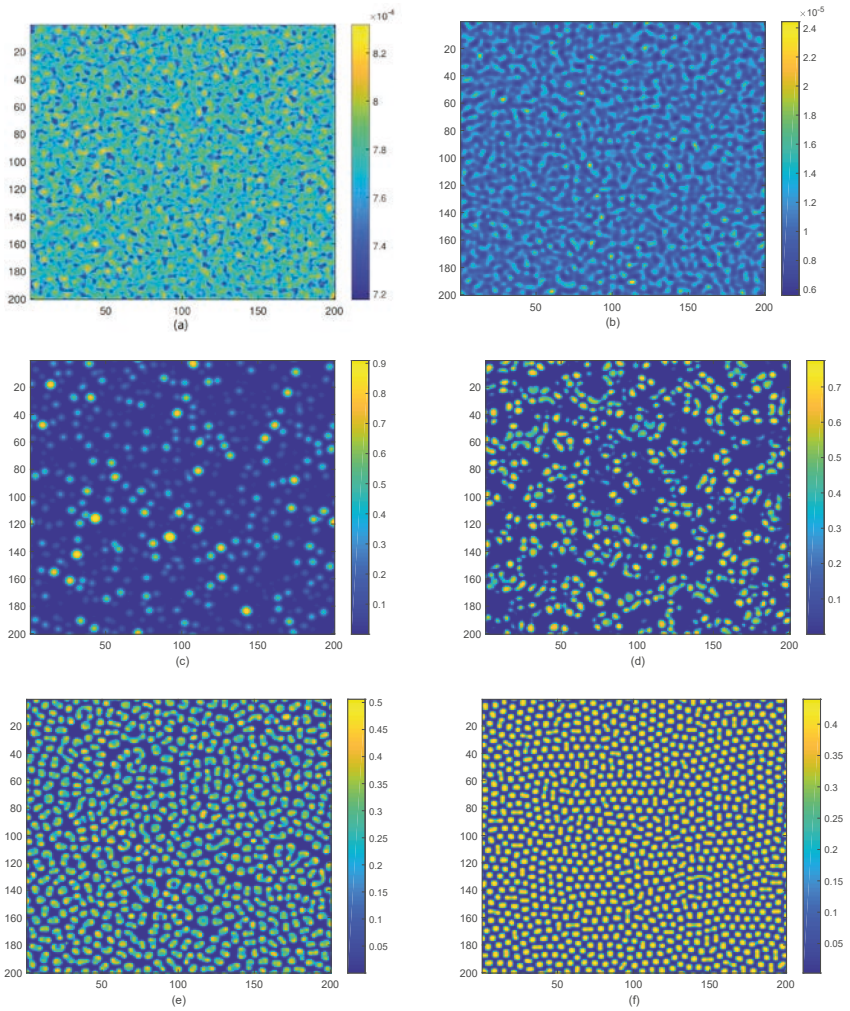


Figure 3. Snapshots of the time evolution profile of the susceptible node u at different moments when $r = 0.2500$ ($\mu \in (\mu_2, \mu_3)$, spot pattern). (a) $t = 3000$; (b) $t = 22500$; (c) $t = 42500$; (d) $t = 70000$; (e) $t = 100000$; (f) $t = 150000$.

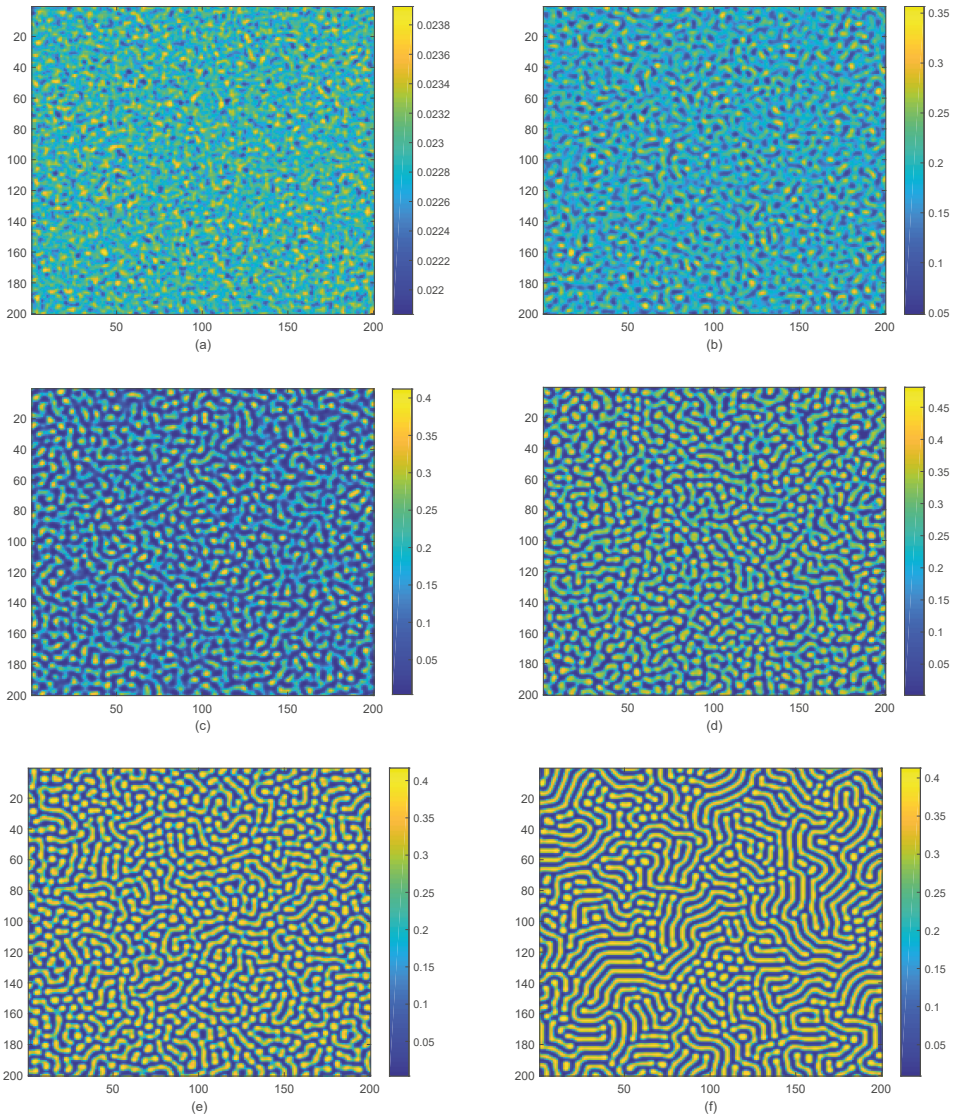


Figure 4. Snapshots of the time evolution profile of the susceptible node u at different moments when $r = 0.2773$ ($\mu \in (\mu_3, \mu_4)$, the mixture of strip and spot pattern). (a) $t = 10000$; (b) $t = 25000$; (c) $t = 37500$; (d) $t = 50000$; (e) $t = 100000$; (f) $t = 150000$.

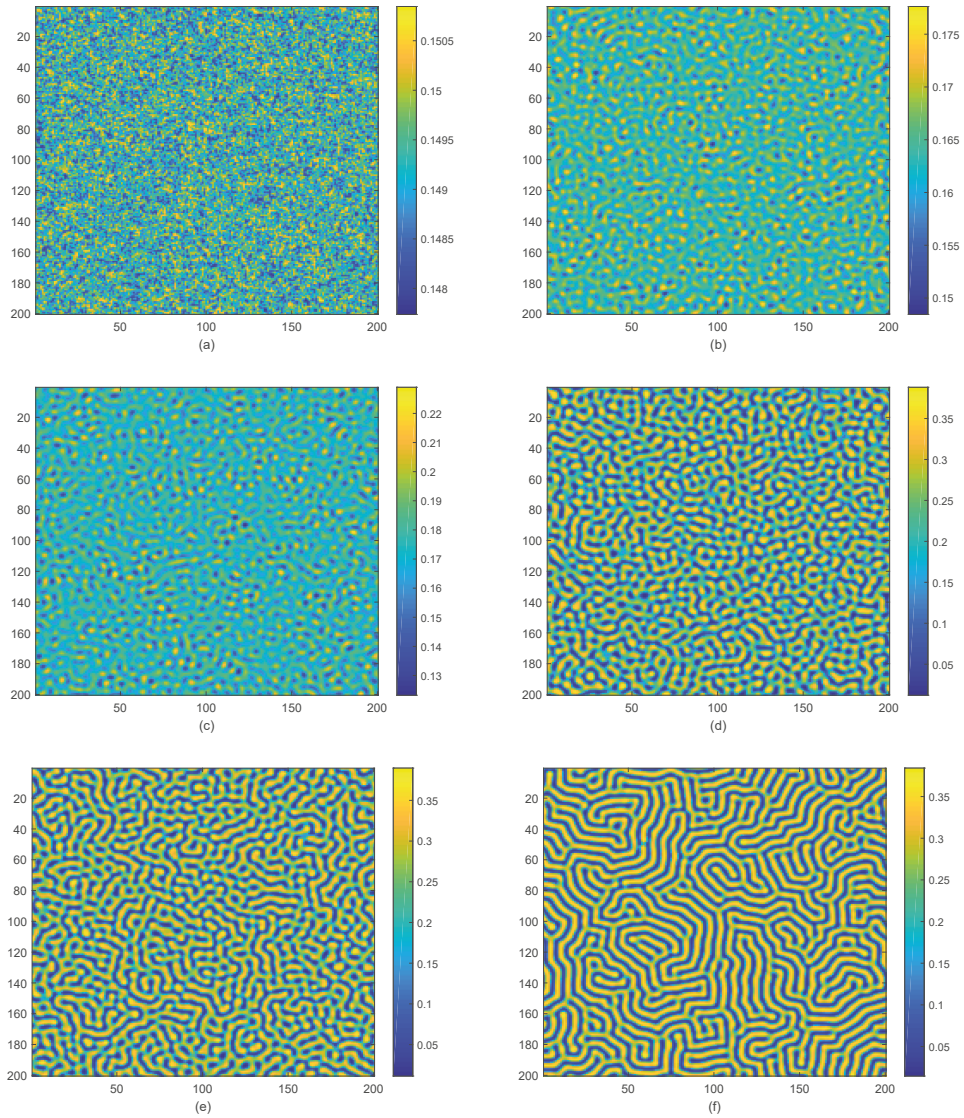


Figure 5. Snapshots of the time evolution profile of the susceptible node u at different moments when $r = 0.3000$ ($\mu > \mu_4$, strip pattern). (a) $t = 2500$; (b) $t = 10000$; (c) $t = 25000$; (d) $t = 37500$; (e) $t = 100000$; (f) $t = 150000$.

mission but also provides a robust mathematical foundation for developing dynamic network security strategies, such as regional isolation and traffic monitoring, to effectively mitigate virus spread. Furthermore, the model's versatility extends beyond computer networks, offering potential applications in interdisciplinary fields such as biological epidemiology and ecological diffusion, where similar pattern formation mechanisms are observed. This work bridges theoretical insights with practical implications, paving the way for future research in both network security and broader scientific domains.

References

[1] J. Amador and J.R. Artalejo. Stochastic modeling of computer virus spreading with warning signals. J. Franklin Inst., 350:1112−1138, 2013.

[2] D. Avcl and F. Soyturk. Optimal control strategies for a computer network under virus threat. J. Comput. Appl. Math., 419:114740, 2023.

[3] A. Bissett and G. Shipton. Some human dimensions of computer virus creation and infection. Int. J. Hum-Comput. Stud., 52:899−913, 2000.

[4] J.Z. Cao, H.Y. Sun, P.M. Hao, and P.G. Wang. Bifurcation and turing instability for a predator-prey model with nonlinear reaction cross-diffusion. Appl. Math. Model., 89: 1663−1677, 2021.

[5] V. Dufiet and J. Boissonade. Dynamics of Turing pattern monolayers close to onset. Phys. Rev. E, 53: 4883−4892, 1996.

[6] B.X. Dai and G.X. Sun. Turing-Hopf bifurcation of a delayed diffusive predator-prey system with chemotaxis and fear effect. Appl. Math. Lett., 111: 106644, 2021.

[7] L.P. Feng, X.F. Liao, H.Q. Li, and Q. Han. Hopf bifurcation analysis of a delayed viral infection model in computer networks. Math. Comput. model, 56: 167−179, 2012.

[8] A. Gierer and H. Meinhardt. A theory of biological pattern formation. Kybernetika, 12: 30−39, 1972.

[9] Z.B. He and X.M. Wang. A spatial-temporal model for the malware propagation in MWSNs based on the reaction-diffusion equations. Inf. Manag., 13: 45−56, 2012.

[10] J.L. Hu, L.H Zhu, and M. Peng. Analysis of Turing patterns and amplitude equations in general forms under a reaction-diffusion rumor propagation system with Allee effect and time delay. Inf. Sci., 596: 501−519, 2022

[11] V. Kumar, N. Kumari, and R.P. Agarwal. Spatiotemporal dynamics and Turing patterns in an eco-epidemiological model with cannibalism. Results Control Optim., 9: 100183, 2022.

[12] M.H.R. Khouzani, S. Sarkar, and E. Altman. Optimal control of epidemic evolution. Proceedings IEEE INFOCOM, 38: 1683−1691, 2011.

[13] Y. Kuramoto and T. Tsuzuki. On the formation of disspipative structures in reaction-diffusion systems. Progr. Theoret. Phys., 54: 687−699, 1975.

[14] X.X. Li, Y.L. Cai, K. Wang, S.M. Fu, and W.M. Wang. Non-constant positive steady states of a host-parasite model with frequency and density-dependent transmissions. J. Franklin Inst., 357: 4392−4413, 2020.

[15] H.C. Liu, B. Ge, and J.H. Shen. Dynamics of periodic solutions in the reaction-diffusion glycolysis model: Mathematical mechanisms of Turing pattern formation. Appl. Math. Comput., 431: 127324, 2022.

[16] A.W. Li, Z. Jin, L. Li, and J.Z. Wang. Emergence of oscillatory turing patterns induced by cross diffusion in a predator-prey system. Int. J. Mod. Phys. B, 26: 1250193, 2012.

[17] Y.F. Luan, M. Xiao, Z. Wang, and J. Zhao. Hybrid control of Turing instability and Hopf bifurcation in CDK1-APC feedback systems with diffusion. J. Franklin Inst., 360: 12170−12197, 2023.

[18] J. Liu and Z.Z Zhang. Hopf bifurcation of a delayed worm model with two latent periods. Adv. Differ. Equ., 442: 1−27, 2019.

[19] E. Makinen. Comment on 'A framework for modelling trojans and computer virus infection'. Comput. J., 44: 321−323, 2001.

[20] V. MadhuSudanan and R. Geetha. Dynamics of epidemic computer virus spreading model with delays. Wirel. Pers. Commun., 115: 2047−2061, 2020.

[21] Q.Y. Qu. Nonlinear Science and The Pattern Dynamics Introduction. Peking University Press, 2010.

[22] Z. Sabir, S.A. Bhat, and M.A.Z. Raja. A swarming neural network computing approach to solve the Zika virus model. Eng. Appl. Artif. Intel., 126: 106924, 2023.

[23] S.V. Stasenko, A.E. Hramov, and V.B. Kazantsev. Loss of neuron network coherence induced by virus-infected astrocytes: a model study. Sci. Rep., 13: 6401, 2023.

[24] J.E. Sawyer, M.C. Kernan, D.E. Conlon, and H. Garland. Responses to the michelangelo computer virus threat: The role of information sources and risk homeostasis theory. J. Appl. Soc. Psychol., 29: 23−51, 1999.

[25] G. Sun, Z. Wu, Z. Jin, and Z. Wang. Influence of isolation degree of spatial patterns on persistence of populations. Nonlinear Dyn., 83: 1−819, 2016.

[26] J.P. Tripathi, S. Abbas, G.Q. Sun, D. Jana, and C.H. Wang. Interaction between prey and mutually interfering predator in prey reserve habitat: Pattern formation and the Turing-Hopf bifurcation. J. Franklin Inst., 355: 7466−7489, 2018.

[27] W.M. Wang, X.Y. Gao, Y.L. Cai, H.B. Shi, and S.M. Fu. Turing patterns in a diffusive epidemic model with saturated infection force. J. Franklin Inst., 355: 7226−7245, 2018.

[28] X.M. Wang, Z.B. He, X.Q. Zhao, C. Lin, Y. Pan, and Z.P. Cai. Reaction-diffusion modeling of malware propagation in mobile wireless sensor networks. Sci. China Inf. Sci., 56: 1−18, 2013.

[29] J.C. Wierman and D.J. Marchette. Modeling computer virus prevalence with a susceptible-infected-susceptible model with reintroduction. Comput. Stat. Data Anal., 45: 3−23,2004.

[30] H. Zhang, R.K. Upadhyay, G.Y. Liu, and Z.Z. Zhang. Hopf bifurcation and optimal control of a delayed malware propagation model on mobile wireless sensor networks. Results Phys., 41: 105926, 2022.

[31] P.T. Zhang, W. Wang, and Y. Tan. A malware detection model based on a negative selection algorithm with penalty factor. Sci. China Inf. Sci., 53: 2461−2471, 2010.

[32] Z. Zhang and H. Yang. Dynamical analysis of a viral infection model with delays in computer networks. Math. Probl. Eng., 2015: 280856, 2015.

[33] L.H. Zhu, H.Y. Zhao, and X.M. Wang. Stability and bifurcation analysis in a delayed reaction-diffusion malware propagation model. Comput. Math. Appl., 69: 852−875, 2015.

[34] L.H. Zhu, H.Y. Zhao, and X.M. Wang. Bifurcation analysis of a delay reaction-diffusion malware propagation model with feedback control. Commun. Nonlinear Sci. Numer. Simul., 22: 747−768, 2015.



Guangyong Zhang received the B.S. degree in Information and Computing Science from Chuzhou University, Anhui, China, in 2013, and the M.S. and Ph.D. degrees in Control Science and Engineering from Jiangsu University, Jiangsu, China, in 2014 and 2021, respectively. Since 2014, he mainly engages in research on the theory and application of nonlinear dynamical systems. From 2021 to present, he was a lecturer of the university with the Department of General Education, Wuxi University, Wuxi, Jiangsu, China. His current research interests include the modeling of nonlinear differential dynamics systems, complex network and time series analysis.
https://orcid.org/0000-0002-9163-0889



Jiahui Zhang received the B.S. degree in Electrical Engineering and Automation from Sanjiang University in 2021, and the M.S. degree in Electronic Information from Nanjing University of Posts and Telecommunications in 2024.She works as an engineer at China Mobile Group Anhui Co., Ltd. Her current research interests include cloud computing and complex systems.
https://orcid.org/0009-0000-2862-9909



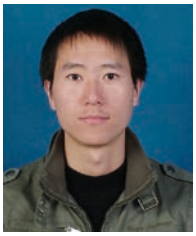
Ludmila Dymova received her Ph.D. in technical sciences from the Samara Technical University in Russia in 1986. In 2012, she obtained the title of Professor of Technical Sciences with a specialization in Computer Science (Poland). The topics of her research activities, in general, may be defined as: "Development of modeling, identification, decision-making, and optimization methods under conditions of objective and non-probabilistic types of uncertainty in economic, technological, and ecological applications." From 1975 to 1999, she worked in Russia and Belarus, since 2000 she has been working at the Częstochowa University of Technology, and since 2023 she has been working at SAN University (Poland). She is the author of more than 150 publications and two books closely related to the subject of her interests.
https://orcid.org/0000-0002-5387-9990



Ying Zhou received the B.S. degree in mathematics education and the M.S. degree in operational and cybernetics research from Qufu Normal University, Qufu, China, in 2000 and 2003, respectively, and the Ph.D. degree in control theory and control engineering from Southeast University, Nanjing, in 2007. She is currently an associate Professor with the College of Automation and College of Artificial Intelligence, Nanjing University of Posts and Telecommunications, Nanjing. Her current research interests include networked control systems, complex systems control, nonlinear adaptive control.
https://orcid.org/0000-0002-7848-4987



Hua Li received the B.S. degree in Measurement and Control Technology and Instruments from the College of Automation, Xian University of Posts and Telecommunications, Shaanxi, China, in 2022. He is currently pursuing the M.S. degree in control science and engineering with the College of Automation and College of Artificial Intelligence, Nanjing University of Posts and Telecommunications, Nanjing, China. His current research interests include complex dynamical systems, nonlinear control theory, partial differential systems, bifurcation, and pattern dynamics.
https://orcid.org/0009-0006-4907-7158



Min Xiao (Senior Member, IEEE) received the B.S. degree in mathematics and the M.S. degree in fundamental mathematics from Nanjing Normal University, Nanjing, China, in 1998 and 2001, respectively, and the Ph.D. degree in applied mathematics from Southeast University, Nanjing, in 2007. He was a Post-Doctoral Researcher or a Visiting Researcher with Southeast University, the City University of Hong Kong, Hong Kong, and Western Sydney University, Sydney, NSW, Australia. He is currently a Professor with the College of Automation and College of Artificial Intelligence, Nanjing University of Posts and Telecommunications, Nanjing. His current research interests include information security, tipping prediction, intelligent logistics systems, and cyber-physical systems.
https://orcid.org/0000-0002-8992-153X